Nano-assemblies with core-forming hydrophobic polypeptide via polymerization-induced self-assembly (PISA)

T. Dao, Lubomir Vezenkov, Gilles Subra, Vincent Ladmiral, M. Semsarilar

Polymer Chemistry

Nano-assemblies with Core-Forming Hydrophobic Polypeptide via Polymerization-Induced Self-Assembly (PISA)

Journal:	*Polymer Chemistry*
Manuscript ID	Draft
Article Type:	Paper
Date Submitted by the Author:	n/a
Complete List of Authors:	Dao, Tuyen; University of Montpellier, IEM Vezenkov, Lubomir; ENSCM, IBMM team 9; Subra, Gilles; Institut des Biomolecules Max Mousseron, Ladmiral, Vincent; Institut Charles Gerhardt - UMR(CNRS), Ingénierie et Architectures Macromoléculaires Semsarilar, Mona; University of Montpellier, IEM

Mona SEMSARILAR, PhD
CNRS Researcher
Institut Européen des Membranes
Université Montpellier
2 place E. Bataillon
34095 MONTPELLIER Cedex 5, France
Mail : mona.semsarilar@umontpellier.fr

Montpellier, 01/06/2020

Dear Editor,

Please find attached our paper entitled "*Nano-assemblies with Core-Forming Hydrophobic Polypeptide via Polymerization-Induced Self-Assembly (PISA)*" for consideration for publication as a full article in *Polymer Chemistry,* Polymerization-Induced Self-Assembly (PISA) special issue.

In recent years polymerization-induced self-assembly (PISA) mediated by reversible addition−fragmentation chain transfer (RAFT) dispersion polymerization has changed the way synthetic chemists prepare and self-assemble block copolymers. PISA is indeed a powerful and versatile technique for the synthesis and self-assembly of a wide range of block copolymer nano-objects of controllable size, morphology, and surface functionality.

The polymers used in PISA have so far been for the vast majority unable to develop supramolecular interactions. Apart from the recent report of Rieger et al (https://doi.org/10.1002/anie.201809370), there are no other study on PISA and supramolecular interactions. In the present manuscript, we take a new approach to the established PISA procedure, and we prepare peptide-polymer hybrids. Two new monomers bearing short peptide sequences capable of self-assembling due to pi-pi stacking and H-bonding were synthesized. We demonstrate that insertion of only few units of these self-assembling peptide (SAP) monomers in the core-forming block of a typical PISA formulation (poly (glycerol monomethacrylate) (PGMA) stabilizing first block followed by dispersion polymerization of 2-hydroxypropyl methacrylate (HPMA)) completely changes the self-assembly regime of this diblock copolymers. New morphologies were observed thus underlining the decisive influence of the SAP monomers.

We believe that the special PISA issue in *Polymer Chemistry* is an ideal platform to report these exciting new results, which should be of considerable interest to polymer chemists as well as material scientists. We would thus be very grateful if you could consider our manuscript for publication.

On behalf of all the co-authors,

Yours sincerely,

Mona Semsarilar

ARTICLE

Nano-assemblies with Core-Forming Hydrophobic Polypeptide *via* Polymerization-Induced Self-Assembly (PISA)

Received 00th January 20xx,
Accepted 00th January 20xx

DOI: 10.1039/x0xx00000x

T. P. Tuyen Dao[a,b,c], Lubomir Vezenkov[c], Gilles Subra[c], Vincent Ladmiral[b], Mona Semsarilar[a*]

Abstract: The aim of this study is to produce self-assembled structures with hydrophobic polypeptide cores *via* Reversible Addition-Fragmentation chain Transfer (RAFT) - mediated Polymerisation-Induced Self-Assembly (PISA). Hydrophilic poly(glycerol monomethacrylate) macromolecular chain transfer agents (PGMA mCTAs) were used to polymerize the self-assembling peptide monomers, resulting in the formation of diblock copolymer nano objects. Methacrylamide derivatives containing self-assembling tripeptide; MAm-GFF (MAm-Gly-Phe-Phe-NH_2) and MAm-FGD (MAm-Phe-Gly-Asp-NH_2) were used as hydrophobic monomers. The self-assembling behaviours of these monomers mainly derive from the interactions of the phenylalanine residues, however their difference in hydrophobicity required different polymerization conditions. MAm-GFF was polymerized in the presence of organic solvent (ethanol or acetonitrile), under either dispersion or emulsion polymerization, while MAm-FGD was polymerized under aqueous dispersion conditions. PGMA-*b*-P(MAm-FGD) obtained from aqueous PISA typically formed fibrous structures while a range of morphologies such as fibre-, flake-, leaf-like or spherical vesicles were obtained for PGMA-*b*-P(MAm-GFF) depending on the copolymer composition and solvent used. In all cases the peptides self-assembling core had a crucial influence on the final morphologies.

Introduction

Self-assembled nanostructures based on polypeptide-polymer hybrid are interesting biomaterials with potential significant impacts in applied biology and medicine. Compared to pure polymeric nanoparticles, these structures could present increased biocompatibility and biofunctionality typical of the peptide sequences,[1-3] in addition to the robustness and functional diversity conferred by the polymer chains. Moreover, the range of self-assembled peptide-containing structures is more diverse than that of polymer nano-objects.[4-6] They can form more complex supramolecular assemblies such as nano-fibers, ribbons, tapes, tubes, wires or rods.[6-15] In particular, since the molecular self-organization of these structures is mainly attributed to weak interactions such as electrostatic forces, hydrophobic interactions, π – π stacking and hydrogen bonding,[16] these structures can largely vary in both shape and size depending on internal or external stimuli (pH, temperature, ionic strength, solvents…).[17-19] The diversity and versatility of peptide-based nanostructures allow them to be potentially used in different biomedical fields such as biosensors, tissue engineering, or drug delivery.[4, 20-23]

Besides the conventional self-assembly strategies using purified and isolated amphiphilic block copolymers, polymerization-induced self-assembly (PISA) has been shown to be a powerful polymer self-assembly method over the last decade and as such has received considerable interest.[24, 25] PISA strategy is fast, eliminating time-consuming steps such as isolation/ purification and redispersion of the amphiphilic polymers since it proceeds *via* the simultaneous formation and self-assembly of the amphiphilic block copolymers.[26] While the conventional post-polymerization methods provide dilute suspensions of nanoparticles (ca. 1% w/w), PISA generates nanoparticles at much higher concentrations (up to 50% w/w as reported in recent studies).[27, 28] Moreover, PISA works well under either dispersion[29-33] or emulsion polymerization conditions[34-37] and in a wide range of solvents.[38-45] Although the use of PISA is drastically growing due to its advantages, most reports show relatively simple self-assembled morphologies (spheres, worms and vesicles).[25] Inspired by the properties of peptide-based nanostructures as well as PISA approach, we have recently reported the first example of PISA nano-objects derived from self-assembling peptide (SAP) containing polymer.[46] The SAP monomer used in this study (MAm-GFF), was a methacrylamide-functionalized GFF tripeptide (GFF = Glycine-Phenylalanine-Phenylalanine). The tripeptide moieties were incorporated along with glycerol monomethacrylate (GMA) in the stabilizing block which was successfully chain extended under PISA conditions with poly(2-hydroxypropyl methacrylate) (PHPMA). The resulting P(GMA_{65}-*stat*-$(MAm\text{-}GFF)_7$)-*b*-$PHPMA_{28}$ diblock copolymer formed fibrous structures in water. Herein, the same peptide methacrylamide was used but as precursor of the core-forming block. PISA formulations with core-forming block composed of copolymer of this SAP

[a.] *Institut Européen des Membranes, IEM, Univ Montpellier, CNRS, ENSCM, Montpellier, France*
[b.] *Institut Charles Gerhardt Montpellier, ICGM, Univ Montpellier, CNRS, ENSCM, Montpellier, France*
[c.] *Institut des Biomolécules Max Mousseron, IBMM , Univ Montpellier, CNRS, ENSCM, Montpellier, France*
Electronic Supplementary Information (ESI) available: NMR spectra, SEC curves, DLS data, digital photos taken, Summary Table for all obtaining products. See DOI: 10.1039/x0xx00000x

methacrylamide and a solvophilic monomer (GMA or HPMA) were also examined. Moreover, a new tripeptide-containing methacrylamide, (MAm-FGD) based on the phenylalanine- glycine-aspartic acid SAP sequence was also studied. As for MAm-GFF, the self-assembly property of MAm-FGD is also attributed to the phenylalanine residue. However MAm-FGD is slightly less hydrophobic than MAm-GFF at physiological pH, and thus allows the use of different PISA conditions. All the synthetic approaches of this work are summarized in Scheme **1**.

Experimental section

Materials

Fmoc-amino acid derivatives (Fmoc-Phe-OH, Fmoc-Gly-OH, Fmoc-Asp(tBu)-OH), HATU (1-[bis(dimethylamino)methylene]-1H-1,2,3-triazolo[4,5-b]pyridinium 3-oxide hexafluorophosphate) and polystyrene Fmoc Rink Amide resins (100-200 mesh) with a loading of 0.94 mmol/g were purchased from Iris Biotech GmbH. Methacrylic acid, piperidine, *N,N*-diisopropylethylamine (DIEA), trifluoroacetic acid (TFA), triisopropylsilane (TIS), glycerol monomethacrylate (GMA), 2-hydroxypropyl methacrylate (HPMA), *4,4'*-azobis(4-cyanopentanoic acid) (ACVA) and all organic solvents were purchased from Sigma-Aldrich. The NMR deuterated solvents (DMSO-d6, methanol-d4 and D_2O) were purchased from Eurisotop. The RAFT agent (4-cyano-4-(2-phenylethanesulfanylthiocarbonyl)-sulfanylpentanoic acid) (PETTC) and the peptide monomer MAm-GFF was prepared according to our previous report.[46]

Scheme 1. Schematic representation of the synthesis of the monomers and block copolymers.

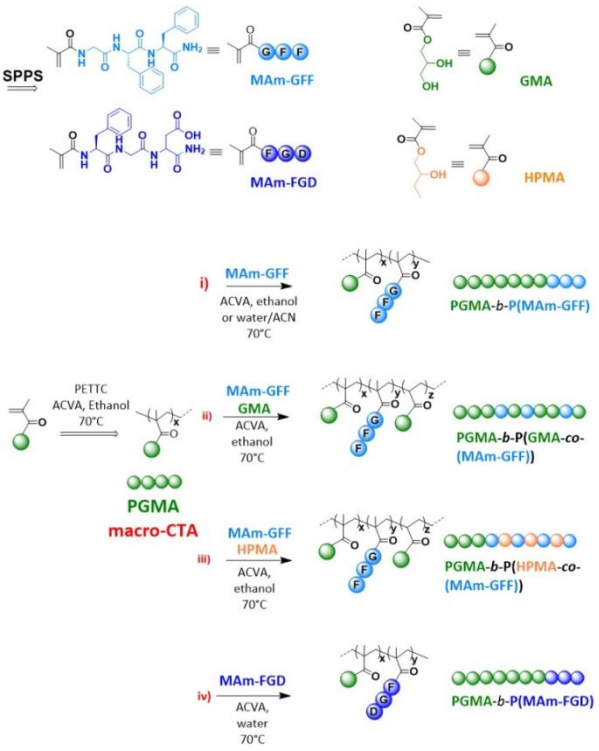

Synthesis of methacrylamide-functionalized peptide monomer MAm-FGD

MAm-FGD was synthesized on the resin using the same protocol employed to make MAm-GFF in our previous report[46] but with Fmoc-Phe-OH, Fmoc-Gly-OH and Fmoc-Asp(But)-OH as the amino acids. At the end, the tripeptide was cleaved from the resin with a TFA/TIS/H_2O (95/2.5/2.5) mixture for 2h at room temperature. It was recovered by precipitation in cold diethyl ether, taken up in water and freeze-dried. The obtained crude white powder was used for polymerisations without any further purification. Its purity and molecular structure were verified by LC-MS (Figure S2) and ^{1}H NMR spectroscopy (Figure S1). ^{1}H NMR in DMSO δ (ppm): 1.85 (s, 3H, -C*H*$_3$); 2.66-2.73 (m, 2H, -CH-C*H*$_2$-Ph); 2.90-3.10 (dd, 2H, -CH-C*H*$_2$-COOH); 3.70 (m, 2H, -NH-C*H*$_2$CO-) 4.41 (m, 2H, -NH-C*H*CO-CH$_2$-); 5.38 (s, 1H, vinyl); 5.71 (s, 1H, vinyl); 7.10-7.28 (m, 5H, phenyl); 8.08-8.20 (m, 3H, -N*H*-).

RAFT Homopolymerization of GMA

A representative synthesis of the PGMA macromolecular chain transfer agents (mCTAs) proceeded as follows: a round bottom Schlenk flask equipped with a stirrer bar was charged with GMA (30 eq.), PETTC (1 eq.), ACVA initiator (0.1 eq.) and a volume of ethanol adjusted for the reaction to proceed at a solids content of 50% w/w. The flask was subsequently sealed with a rubber septum, placed in an ice-bath, degassed by bubbling nitrogen for 30 min and immersed in a preheated oil bath at 70°C. After 2h, the polymerization was quenched by immersing the flask in ice-cold water and opening the reaction to air. GMA conversion was determined by ^{1}H NMR in methanol-d4, from the ratio of the integral of the residual vinyl ^{1}H signals at 5.65 ppm (1H) or 6.15 ppm (1H) to the signals at 3.5-4.3 (5H). The mixture reaction was then dialyzed using a MWCO = 1kDa membrane against a 9/1 mixture of water and ethanol during two days and freeze-dried. The final product was a light yellow powder. The mean DP was determined by ^{1}H NMR and the molar mass distribution was determined using DMAc SEC. All the ^{1}H NMR spectra and SEC chromatograms of the PGMA mCTAs are provided in Figure S3-S6.

Preparation of diblock PGMA$_x$-*b*-P(MAm-GFF)$_y$ *via* RAFT-PISA using PGMA$_x$ as mCTA

PGMA$_x$ mCTA (1 eq.), MAm-GFF (y eq.), and ACVA (0.2 eq.) were charged into a 10-mL glass vial and stirred with the chosen polymerization solvent. The vial was sealed, submerged in an ice-bath, degassed for 30 minutes and put into an oil-bath set previously at 70°C. After 24h, reaction was cooled down, opened to the air and the MAm-GFF conversion was determined by ^{1}H NMR (comparison of the integral of the residual vinyl signals at 5.42 (1H) or 5.85 (1H) to that of the phenyl group at 7.2-7.4 (10H)). Other aliquots were also taken for SEC, DLS and TEM analyses.

Preparation of diblock PGMA$_{18}$-*b*-P((MAm-GFF)$_9$-*co*-GMA$_{48}$) *via* RAFT-PISA using PGMA$_{18}$ as mCTA

The procedure to prepare $PGMA_{18}$-*b*-P((MAm-GFF)$_9$-*co*-GMA_{48}) using $PGMA_{18}$ as mCTA was as follows: $PGMA_{18}$ mCTA (1 eq.), MA-GFF (10 eq.) GMA (48 eq.) and ACVA (0.2 eq.) were stirred with pure ethanol into a 10-mL glass vial. The vial was subsequently sealed with a rubber septum, submerged in an ice-bath, degassed by bubbling nitrogen for 30 min and immersed in a preheated oil bath at 70°C. After 24h, the reaction was quenched by cooling and exposing to air. MAm-GFF conversion was determined as described above while GMA conversion was always 100% (no remaining GMA-vinyl signals). Other aliquots were also taken for SEC, DLS and TEM analyses.

Preparation of diblock $PGMA_{18}$-*b*-P((MAm-GFF)$_9$-*co*-$HPMA_{61}$) and $PGMA_{18}$-*b*-P((MAm-GFF)$_{19}$-*co*-$HPMA_{50}$) *via* RAFT-PISA using $PGMA_{18}$ as mCTA

The procedures were as follow: $PGMA_{18}$ mCTA, MA-GFF, HPMA and ACVA at ratio 1 : 10 : 61 : 0.2 (to prepare $PGMA_{18}$-*b*-P((MAm-GFF)$_9$-*co*-$HPMA_{61}$) and 1 : 20 : 50 : 0.2 (to prepare $PGMA_{18}$-*b*-P((MAm-GFF)$_{19}$-*co*-$HPMA_{50}$)) were stirred with ethanol into a 10-mL glass vial. The vial was subsequently sealed with a rubber septum, submerged in an ice-bath, degassed by bubbling nitrogen for 30 min and immersed in a preheated oil bath at 70°C. After 24h, the reaction was quenched by exposing to air. MAm-GFF conversion was determined as same as described above while HPMA conversion was always 100% (no remaining HPMA-vinyl signals). Other aliquots were also taken for SEC, DLS and TEM analyses.

Preparation of diblock $PGMA_x$-*b*-P(MAm-FGD)$_y$ *via* RAFT-PISA using $PGMA_x$ as mCTA

The typical procedure of RAFT-PISA to prepare diblock $PGMA_x$-b-P(MAm-FGD)$_y$ using $PGMA_x$ as mCTA was carried out as described below. $PGMA_x$ mCTA (1 eq.), MAm-FGD (y eq.), ACVA (0.2 eq.) and water (to reach 10% w/w of solids content) were charged into a 10-mL glass vial. The vial was sealed, degassed for 30 minutes and put into an oil-bath set previously at 70°C. After 24h, reaction was cooled down, opened to the air and the MAm-FGD conversion was determined by ^{1}H NMR (comparison of its residual vinyl signals at 5.42 (1H) or 5.85 (1H) to the phenyl group at 7.2-7.4 (5H)). Other aliquots were also taken for SEC, DLS and TEM analyses.

Characterization

Liquid chromatography – mass spectrometry (LC-MS): LC-MS analyses were performed on Waters Alliance 2695 HPLC system, coupled to a Water Micromass ZQ spectrometer (electrospray ionization mode, ESI+). The peptide monomer MAm-GFF was dissolved in a minimum amount of DMF and diluted with acetonitrile/water (50/50 v/v) mixture containing 0.1% TFA. UV detection was performed at 214 nm.

Proton nuclear magnetic resonance spectroscopy (^{1}H NMR): ^{1}H NMR spectra were recorded on a 300 MHz Bruker Avance-300 spectrometer, processed and analyzed with MestReNova 9.0.

Size exclusion Chromatography (SEC): Polymer molar mass distributions were analysed using GPC Varian 390-LC system with PL1113-6300 ResiPore 300 x 7.5 columns connected with 390LC PL0390-0601 refractive index detector (RI). The mobile phase was DMAc with 0.1% w/w LiBr adjusted at a flow rate of 1mL min^{-1} while the columns were thermostated at 70°C. The calibration was done with near-monodisperse Poly(methyl methacrylate) (PMMA) standards ranging from 550 to 1 568 000 g mol^{-1} (EasiVial-Agilent).

Dynamic light scattering (DLS): The hydrodynamic radii RH were analysed by dynamic light scattering at 90° using Litesizer TM 500 Anton Paar. All measurements were performed at 20°C and with samples diluted to 0.1% w/w.

Transmission Electron Microscopy (TEM): TEM images were acquired using either JEOL 1200 EXII-120 kV or JEOL 1400 P+ - 120 kV. To prepare the TEM grid, 10 µL of 100-fold diluted sample from PISA suspension (0.1% w/w) was deposited onto the grid for 60s and then blotted with filter paper to remove excess solution. Afterward, the sample-loaded grid was stained with 7 µL of 1% ammonium molybdate solution for 20s and also removed the excess stain with filter paper. The grid was allowed to dry under the hood for 5 minutes.

Results and discussion

PGMA macromolecular chain transfer agents (PGMA mCTAs)

The homopolymerizations of GMA were performed in ethanol under solution polymerization conditions. Although almost full conversion could be reached in 5h as shown in previous studies,[47] in this work, the polymerizations of GMA were stopped at about 60% conversion to ensure good end-group fidelity. The DP of the resulting PGMA mCTAs (18, 40 and 83 for mCTAs **1**, **2**, and **3** respectively, Figure S3-5) were determined by ^{1}H NMR using the integrals of the signals of the backbone of PGMA (0.8-2 ppm, 5H) and of those of the PETTC end-group (7.2–7.4 ppm, 5H). All three mCTAs had narrow molar mass distributions (Đ = 1.16, 1.21 and 1.27) as judged by SEC in DMAc. SEC traces of these PGMA mCTAs are shown in Figure S6.

PISA using the GFF-functionalized methacrylamide (MAm-GFF)

The polymerizations of MAm-GFF using PGMA mCTAs to prepare self-assembled structures with P(MAm-GFF) as core-forming block were performed in different media containing organic solvents since MAm-GFF is only sparingly soluble in pure water. Common good solvents for hydrophobic peptides are DMF, DMSO, acetonitrile and ethanol. DMF and DMSO could not be used here, as they are both good solvent for P(MAm-GFF). Direct visual observation suggested that in ethanol, MAm-GFF was soluble up to 0.4% w/w at ambient temperature (ca. 20°C) and up to 5% w/w at 70°C. At higher concentrations (7% - 10% w/w), it formed emulsion at both 20 and 70°C. Furthermore, a mixture of water/acetonitrile was also chosen to study as the reaction medium. It was found that in water/acetonitrile 1/2 v/v mixture, MAm-GFF is dispersed up to 10% w/w at both 20°C and 70°C, whereas in water/acetonitrile 1/1 v/v mixture, a 10% w/w MAm-GFF formed an emulsion at 20°C and a solution at 70°C. TEM images of MAm-GFF-derived structures prepared in the above media at low concentration (0.1% w/w) are presented in Figure 1.

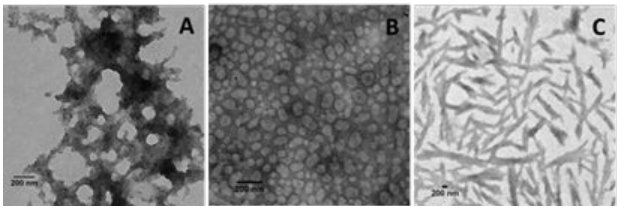

Figure 1. Representative TEM images of MAm-GFF-derived structures prepared from solutions at c = 0.1% w/w in: (A) water/acetonitrile 1/2 v/v; (B) water/acetonitrile 1/1 v/v and (C) ethanol.

In the water/acetonitrile 1/2 v/v mixture, only ill-defined aggregates were observed (Figure 1A), suggesting that MAm-GFF was completely solubilized. However, in mixture of water/acetonitrile 1/1 v/v or in ethanol, MAm-GFF self-assembled into relatively well-defined vesicular morphologies, (Figure 1B) and bundles of short fibers (Figure 1C). As discussed already in our previous work,[46] the self-assembly of MAm-GFF is attributed to the combination of hydrogen bonding and aromatic π-stacking interactions between the FF moieties. The final morphologies thus are not only determined by MAm-GFF molecular structure but also by the solvent quality (polarity and hydrogen bonding properties). This was indeed illustrated here: changing the solvent from ethanol to water/acetonitrile 1/1 v/v mixture provides two types of distinct structures: fibres and vesicles.

These preliminary results on the solution properties of MAm-GFF allowed its use in PISA formulation as the core-forming building block (scheme **1)**.

PISA in ethanol

Solids content effect: A series of polymerisation carried out in ethanol using mCTA **1** ($PGMA_{18}$): an initial ratio of **1**: MAm-GFF: ACVA of 1: 5: 0.2, for 24 h at 70 °C, at various solids content was performed. At 5% w/w, the reaction proceeded under dispersion polymerization, however above 10% w/w, the reaction became an emulsion polymerization. Surprisingly, only 45% MAm-GFF conversion could be attained at 5% w/w solids whereas at 11.2% w/w solids, MAm-GFF conversion reached 87%. This trend was confirmed by a third experiment carried out at 12.5% w/w solids (targeting a DP of P(MAm-GFF) of 10) which reached 92% MAm-GFF conversion. The DMAc SEC traces (Figure 2) of the resulting $PGMA_{18}$-*b*-$P(MAm\text{-}GFF)_x$ diblock copolymers confirmed the relative good control of the RAFT polymerizations. However, a significant shoulder corresponding to the mCTA can be seen on the trace of the $PGMA_{18}$-*b*-$P(MAm\text{-}GFF)_9$ block copolymer, suggesting a suboptimal blocking efficiency.

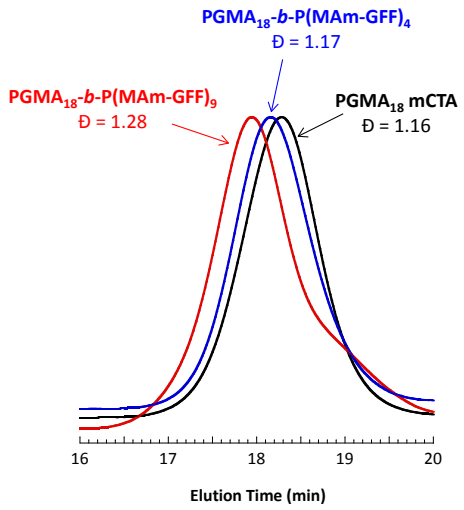

Figure 2. DMAc SEC chromatograms (refractive index detector) for mCTA **1** ($PGMA_{18}$) and the diblock copolymers $PGMA_{18}$-*b*-$P(MAm\text{-}GFF)_4$ and $PGMA_{18}$-*b*-$P(MAm\text{-}GFF)_9$ prepared *via* RAFT-mediated PISA at 70°C in ethanol at 11.2% w/w and 12.5% w/w respectively.

In all cases, at 70°C, the final reaction mixtures were turbid yellow suspensions. However, upon cooling, both suspensions were unstable. They became more turbid and yellow solids were observed on the wall of the vial at ambient temperature, even under continuous stirring, as shown in Figure S7. However, after dilution (100-fold) of the suspensions at 70 °C for TEM and DLS analyses, the samples remained stable at 20°C. TEM images of the $PGMA_{18}$-*b*-$P(MAm\text{-}GFF)_4$ diblock copolymer revealed the formation of flake-like objects about 50 nm wide and 100-200 nm long. In comparison, the $PGMA_{18}$-*b*-$P(MAm\text{-}GFF)_9$ diblock copolymer formed micrometric branched bundles of fibers (Figure 3). In agreement with TEM results, DLS experiments indicated the presence of nano-objects in $PGMA_{18}$-*b*-$P(MAm\text{-}GFF)_4$ suspension with narrow size distribution (PDI = 0.187). Meanwhile, the DLS histogram of $PGMA_{18}$-*b*-$P(MAm\text{-}GFF)_9$ showed the existence of large

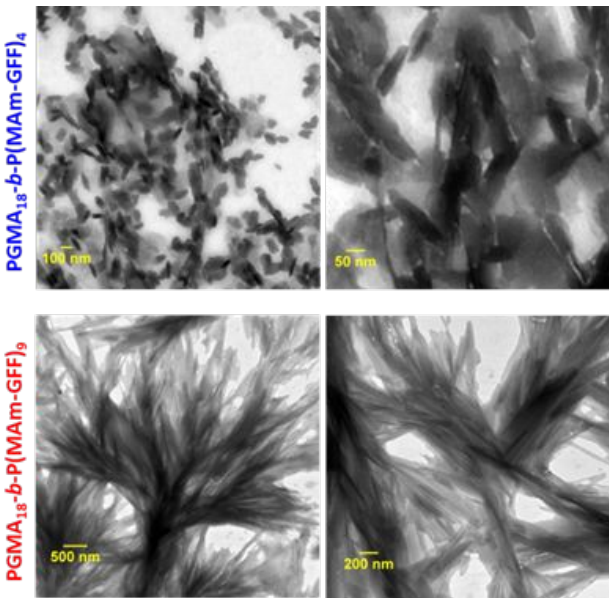

Figure 3. Representative TEM images at different magnification of the $PGMA_{18}$-*b*-$P(MAm\text{-}GFF)_4$ (top row) and $PGMA_{18}$-*b*-$P(MAm\text{-}GFF)_9$ (bottom row) diblock copolymers morphologies prepared by RAFT-PISA in ethanol at 11.2% and 12.5% solids content respectively. Samples were diluted 100-fold at 70°C.

structures at the micrometric scale. The size distribution in this case was broad, probably due to its highly anisotropic morphology as seen with TEM. DLS data are presented in Figure S8. The significant change in both size and shape between the two diblocks ($PGMA_{18}$-*b*-P(MAm-GFF)$_4$ and $PGMA_{18}$-*b*-P(MAm-GFF)$_9$) indicated that the length of the hydrophobic SAP block P(MAm-GFF) effectively determines the final morphology of the PGMA-*b*-P(MAm-GFF) block copolymer. This result confirms the interplay and synergy between SAP and PISA in the formation of these morphologies.

Effect of the mCTA length

To overcome the instability, observed at 20°C for the previous diblock copolymer morphologies, stabilized by a relatively short $PGMA_{18}$, longer hydrophilic mCTAs: $PGMA_{40}$ (**2**) and $PGMA_{83}$ (**3**) were used. All the PISA formulations were carried out at 12% w/w solids in ethanol. The polymerization led to yellow turbid suspensions after 24h. In these polymerizations, MAm-GFF conversions reached 90% or higher as judged by ^{1}HNMR and SEC analyses. However, the resulting diblock copolymers ($PGMA_{40}$-*b*-P(MAm-GFF)$_8$, $PGMA_{83}$-*b*-P(MAm-GFF)$_{10}$ and $PGMA_{83}$-*b*-P(MAm-GFF)$_6$) suspensions again lost their colloidal stability upon cooling from 70°C to 20 °C. Increasing the length of the PGMA block did not improve the stability of PGMA-*b*-P(MAm-GFF) self-assembled objects. Here, the balance between the hydrophobic and hydrophilic parts in the PGMA-*b*-P(MAm-GFF) system was not the dominant element in the self-assembly in contrast to the case of PGMA-*b*-PHPMA which have been thoroughly described.[48] The morphologies observed here were likely more affected by the self-assembling properties of the polypeptide part.

The diblock copolymer morphologies were observed by TEM using 100-fold diluted samples. The dilution was carried out at 70°C. Well-defined morphologies were observed for all PISA formulations as shown in Figure 4. In all cases, despite the composition difference, the self-assembled morphologies were large (several µm) dendritic structures similar to the structures observed for **$PGMA_{18}$-*b*-P(MAm-GFF)$_9$, and** composed of fibrous elements (Figure 4). These fibrous substructures were better defined for the diblocks prepared from the longer $PGMA_{83}$ mCTA. Increasing the length of the P(MAm-GFF) block from 6 to 10 for these $PGMA_{83}$-derived block copolymers led to even better defined fibrous substructures (Figure 4). When $PGMA_{40}$ was used as the stabilizing block, these substructures lost much of their fiber-like aspect.

Effect of the composition of the core-forming block

The effect of the composition of the solvophobic block was also examined by replacing the P(MAm-GFF) segment by a copolymer of HPMA (or GMA) and MAm-GFF. GMA and HPMA are highly soluble in ethanol. Three PISA formulations based on mCTA **1** were examined: **1**: GMA: MAm-GFF = 1: 48: 10, **1**: HPMA: MAm-GFF = 1: 61: 10, and **1**: HPMA: MAm-GFF = 1: 50: 20. The addition of GMA or HPMA increased the solubility of MAm-GFF in the reaction medium, and thus the PISA could be carried out at higher solids contents (15% w/w) which led to higher monomer conversions. The SEC chromatograms of the resulting diblock copolymers shown in Figure 5 suggest that the PISA copolymerizations proceeded with relatively good control (the trace are monomodal and shifted towards higher

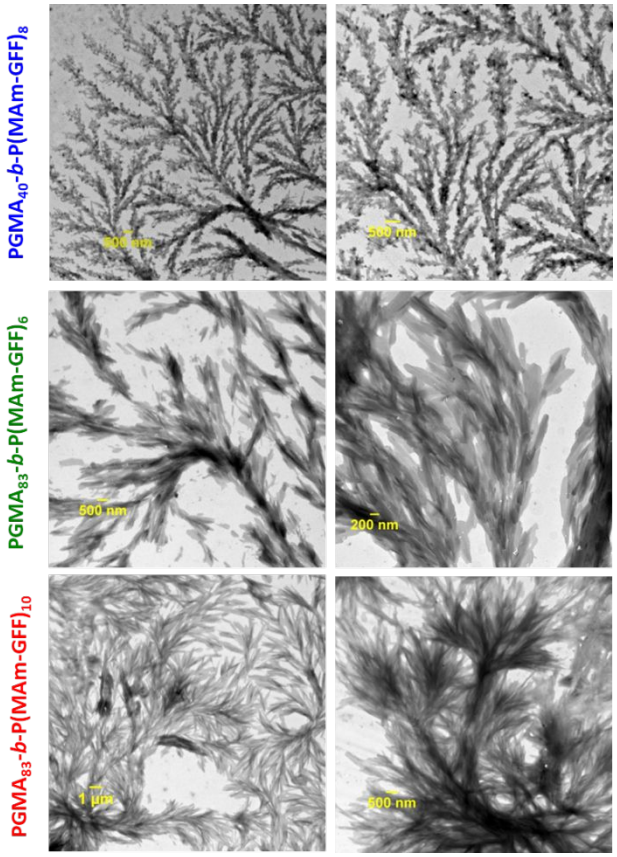

Figure 4. Representative TEM images of the $PGMA_{40}$-*b*-P(MAm-GFF)$_8$, $PGMA_{83}$-*b*-P(MAm-GFF)$_6$ and $PGMA_{83}$-*b*-P(MAm-GFF)$_{10}$ diblock copolymers morphologies prepared **RAFT PISA in emulsion in ethanol** at 12% solids. **The samples were diluted to 0.1% w/w at 70°C.**

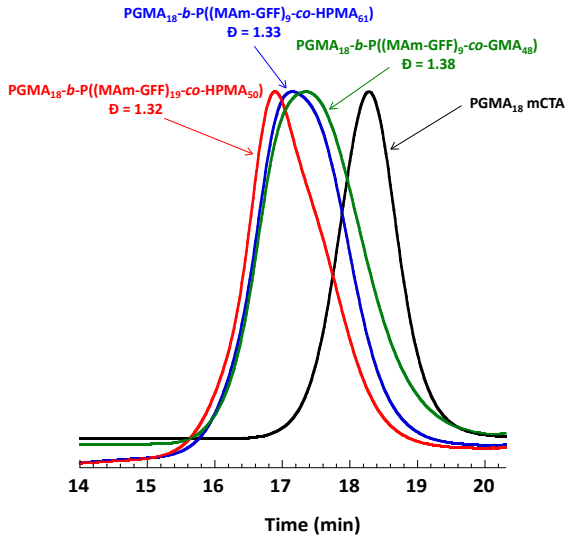

Figure 5. DMAc SEC chromatograms (refractive index detector) for mCTA **1** ($PGMA_{18}$) and the three diblock copolymers prepared by RAFT PISA in emulsion in ethanol.

molar masses). However, these chromatograms were also slightly broad suggesting a subpar blocking efficiency.

As in the case of the previous formulations described above, the suspension of $PGMA_{18}$-*b*-P((MAm-GFF)$_9$-*co*-GMA_{48}) diblock copolymer was turbid and stable at 70°C but rapidly lost colloidal stability in a few minutes after cooling down (Figure S9). TEM images of the sample diluted at 70°C showed large clusters of fibrous structures. In contrast, the $PGMA_{18}$-*b*-P((MAm-GFF)$_9$-*co*-$HPMA_{61}$) and $PGMA_{18}$-*b*-P((MAm-GFF)$_{19}$-*co*-$HPMA_{50}$) diblock copolymers suspensions were colloidally stable at both 70°C and 20°C. The TEM images of these morphologies (samples prepared at 20°c) show that $PGMA_{18}$-*b*-P((MAm-GFF)$_{19}$-*co*-$HPMA_{50}$) self-assembled into vesicles while $PGMA_{18}$-*b*-P((MA-GFF)$_9$-*co*-$HPMA_{61}$) self-assembled into a mixture of short worms and vesicles (Figure 6). It is worth noticing here that these vesicles are undoubtedly the results of the self-assembling properties of MAm-GFF since PGMA-*b*-PHPMA block copolymers are completely soluble in ethanol.

Solvent effect

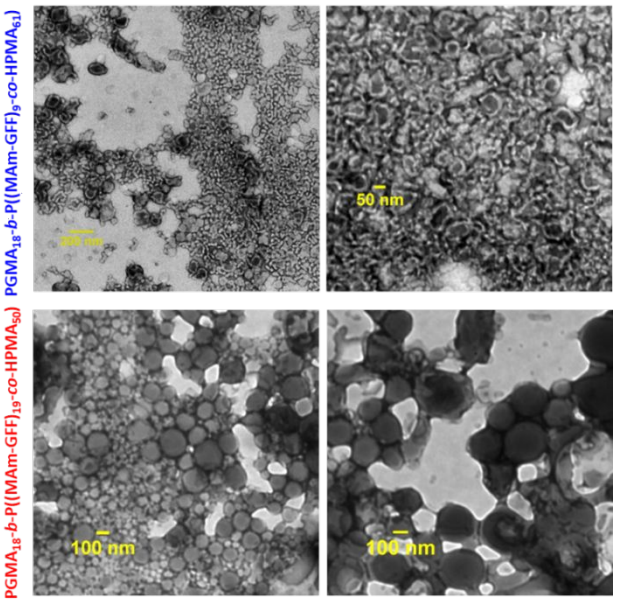

Figure 6. Representative TEM images of the $PGMA_{18}$-*b*-P((MAm-GFF)$_9$-*co*-$HPMA_{61}$) diblock copolymer morphology (top row) and of the $PGMA_{18}$-*b*-P((MAm-GFF)$_{19}$-*co*-$HPMA_{50}$) diblock copolymer morphology (bottom row) prepared by RAFT PISA in dispersion in ethanol at 15% w/w solids. **The samples were diluted to** 0.15% w/w at 20°C.

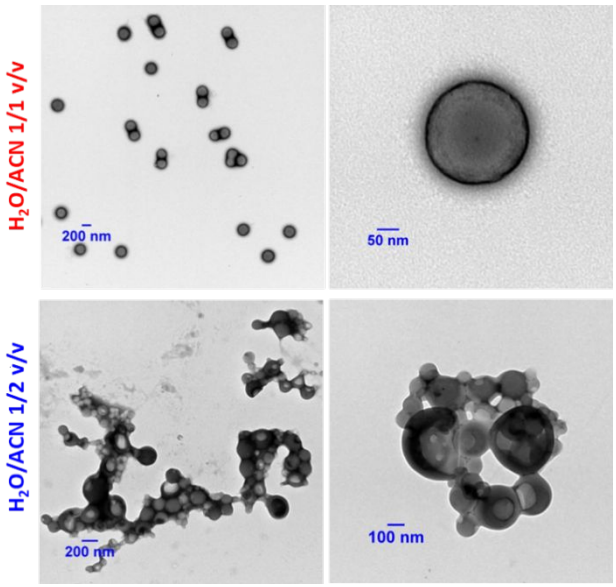

Figure 7. Representative TEM images of the $PGMA_{40}$-*b*-P(MAm-GFF)$_{15}$ diblock copolymer morphology in 1/1 v/v (top row) and (1/2 v/v) (bottom row) water/acetonitrile mixtures prepared by RAFT PISA in dispersion at 10% w/w solids at 70°C. **The samples were diluted to** 0.1% w/w.

The effect of the solvent on the PISA of PGMA-*b*-P(MAm-GFF) diblock copolymer was investigated, and ethanol was replaced by water/acetonitrile mixtures. The following PISA formulation based on mCTA **2** was examined: **2**: MAm-GFF: ACVA = 1: 20: 0.2 in 1/1 v/v and 1/2 v/v water/acetonitrile mixtures. The polymerizations were carried out at 10 w/w solids under RAFT dispersion polymerization conditions at 70°C. The MAm-GFF conversions reached 69% and 72% in 1/1 v/v and 1/2 v/v water/acetonitrile mixtures respectively. **Formation of the diblock copolymers *via* successful chain extension of the macro-CTA with P(MAm-GFF) was confirmed by SEC DMAc as shown in Figure S10.** The resulting diblock copolymer morphologies were well-dispersed, giving rather clear colloidal suspensions that remained colloidaly stable even upon cooling to 20°C. TEM images (Figure 7) showed that $PGMA_{40}$-*b*-(MAm-GFF)$_{15}$ formed monodisperse 220 nm spherical particles in water/acetonitrile 1/1 v/v. In water/acetonitrile 1/2 v/v the PISA of $PGMA_{40}$-*b*-(MAm-GFF)$_{15}$ led to polydisperse vesicles with diameters ranging between 50 and 400 nm. In contrast to the PISA experiments carried out in ethanol which resulted in unstable dispersions and fibrous structures, no fibrous structures were observed for PGMA-*b*-P(MAm-GFF) in the two water/acetonitrile mixtures examined. It is however important to note that the diblock copolymers prepared in ethanol and in water/acetonitrile were not strictly identical. So the difference in their morphologies may not be ascribed only to the effect of solvent.

PISA using GFD-functionalized methacrylamide (MAm-FGD)

In order to perform PISA under aqueous dispersion conditions, a new peptide-functionalized methacrylamide, MAm-FGD, was designed. This monomer, reported for its self-assembling properties, similar to MAm-GFF contains a phenylalanine residue, however it is less hydrophobic as it also contains a polar aspartic

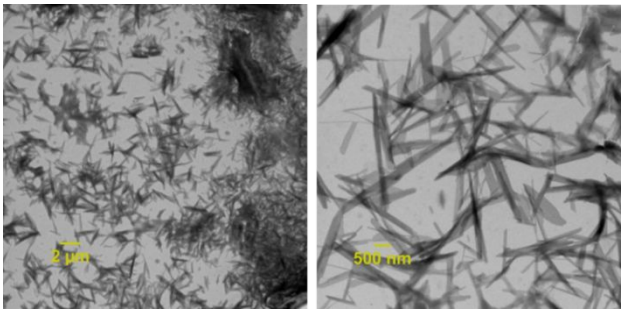

Figure 8. Representative TEM images of self-assembled structures of MAm-FGD in water at 0.1% w/w.

acid unit instead of a second phenylalanine moiety. Indeed, MAm-FGD was soluble in water up to 10% w/w. The TEM images (Figure **8**) of the MAm-FGD aqueous solution at 0.1% w/w revealed the presence of long (several µm) shard–like structures with width in the 100 - 200 nm range that sometimes aggregated into bundles. These TEM images confirmed that a single phenylalanine unit can also drive self-assembly and lead to the formation of fibrous structures, as demonstrated by Gazit et al. [49]

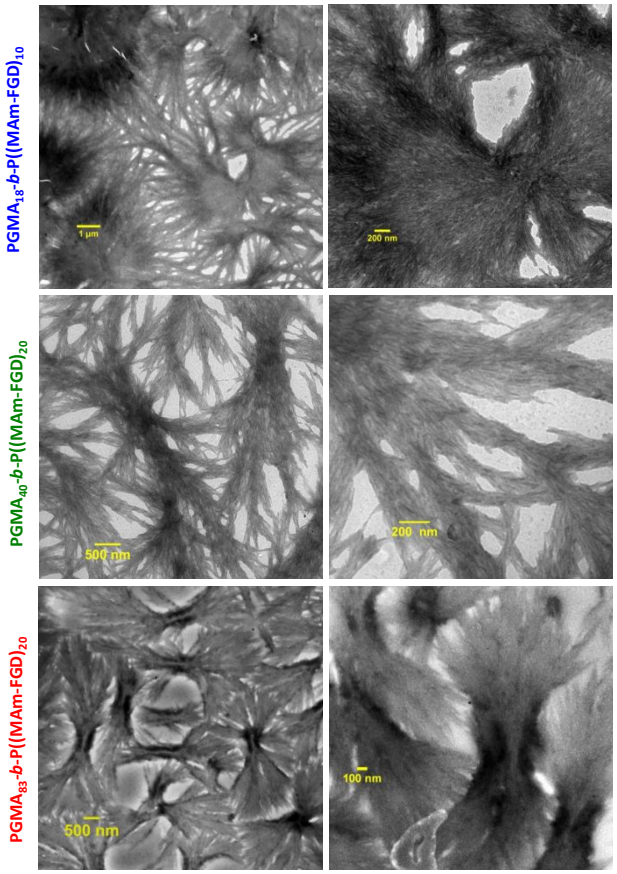

Figure 9. Representative TEM images at different magnification of the $PGMA_{18}$-*b*-$P(MAm\text{-}FGD)_{10}$ (top row), $PGMA_{40}$-*b*-$P(MAm\text{-}FGD)_{20}$, (medium row) and $PGMA_{83}$-*b*-$P(MAm\text{-}FGD)_{20}$ (bottom row) diblock copolymer morphologies prepared by RAFT PISA aqueous dispersion at 10% w/w solids. The samples were diluted to 0.1% w/w.

Polymerizations of MAm-FGD were performed using mCTAs **1, 2** and **3** at 10% w/w solids in water. In all cases, 100% MAm-FGD conversion were achieved and a yellow turbid suspension was obtained. Three diblock copolymers were thus prepared: **$PGMA_{18}$-*b*-$P(MAm\text{-}FGD)_{10}$, $PGMA_{40}$-*b*-$P(MAm\text{-}FGD)_{20}$ and $PGMA_{83}$-*b*-$P(MAm\text{-}FGD)_{20}$**. All three samples formed colloidally stable suspensions at both 70°C and 20°C. TEM images of these suspensions revealed the formation of large dendritic and bow-tie shaped fibrous spherulitic structures (Figure **9**). Although the overall shape is similar for all the compositions, indicating similar organization, a closer look at their internal structures reveals slight differences as seen in images at higher magnifications. From **$PGMA_{18}$-*b*-$P(MAm\text{-}FGD)_{10}$, $PGMA_{40}$-*b*-$P(MAm\text{-}FGD)_{20}$ to $PGMA_{83}$-*b*-$P(MAm\text{-}FGD)_{20}$**, it seems that the fibers become shorter and the structures tend to be less packed.

Conclusions

Nanostructures constituted of a solvophilic PGMA corona and peptide-containing solvophobic cores were successfully prepared *via* RAFT-mediated Polymerization-Induced-Self-assembly using SAP-functionalized methacrylamide. The self-assembly of these polymer-polypeptide formulations proved to be much more diverse compared to the polymeric nano-objects reported in previous PISA works. PISA formulations based on PGMA-*b*-P(MAm-GFF) or PGMA-*b*-P(MAm-FGD) formed large spherulitic bundles of fibrous structures in ethanol and water respectively. In contrast, only spherical particles and vesicles were observed for PGMA-*b*-P(MAm-GFF) synthesized *via* PISA in dispersion in water/acetonitrile mixtures. As observed in our previous work[46] the introduction of only few SAP residues was necessary to greatly influence the self-assembled morphology. This observation further strengthens our hypothesis that PISA and SAP motifs can synergistically contribute to the formation of nano- and micrometric morphologies.

Conflicts of interest

There are no conflicts to declare.

Acknowledgements

PDRA fellowship managed by the French national research agency (ANR): “investissement d’Avenir” LabEX CheMISyst, grant number ANR-10-LABX-05-01. The authors also thank CNRS for funding this work via the “Osez l’interdisciplinarité” programme awarded to MS.

Notes and references

1. J. Shu, B. Panganiban and T. Xu, *Annual review of physical chemistry*, 2013, **64**, 631-657.
2. V. Mikhalevich, I. Craciun, M. Kyropoulou, C. G. Palivan and W. Meier, *Biomacromolecules*, 2017, **18**, 3471-3480.

3. E. Radvar and H. Azevedo, *Macromolecular Bioscience*, 2018, **19**, 1800221.
4. N. Habibi, N. Kamaly, A. Memic and H. Shafiee, *Nano Today*, 2016, **11**, 41-60.
5. D. Mandal, A. Shirazi and K. Parang, *Organic & biomolecular chemistry*, 2014, **12**, 3544-3561.
6. J. Ryu and C. Park, *Biotechnology and bioengineering*, 2010, **105**, 221-230.
7. C. Görbitz, *Chemical communications (Cambridge, England)*, 2006, **22**, 2332-2334.
8. S. Marchesan, A. Vargiu and K. Styan, *Molecules (Basel, Switzerland)*, 2015, **20**, 19775-19788.
9. L. Adler-Abramovich, D. Aronov, P. Beker, M. Yevnin, S. Stempler, L. Buzhansky, G. Rosenman and E. Gazit, *Nature nanotechnology*, 2009, **4**, 849-854.
10. M. Reches and E. Gazit, *Nano Lett*, 2004, **4**, 581-585.
11. M. Reches and E. Gazit, *Physical biology*, 2006, **3**, S10-19.
12. R. Huang, W. Qi, R. Su, J. Zhao and Z. He, *Soft Matter*, 2011, **7**, 6418.
13. C. Guo, Y. Luo, Z. Ruhong and G. Wei, *Nanoscale*, 2014, **6**, 2800-2811.
14. M. Reches and E. Gazit, *Science (New York, N.Y.)*, 2003, **300**, 625-627.
15. H. Arakawa, K. Takeda, S. Higashi, A. Shibata, Y. Kitamura and M. Ikeda, *Polymer Journal*, 2020, DOI: 10.1038/s41428-019-0301-5, 1-8.
16. S. Stupp, *Nano letters*, 2010, **10**, 4783-4786.
17. J. Wang, K. Liu, R. Xing and X. Yan, *Chemical Society reviews*, 2016, **45**, 5589-5604.
18. A. Mendes, E. Baran, R. L. Reis and H. Azevedo, *Wiley interdisciplinary reviews. Nanomedicine and nanobiotechnology*, 2013, **6**, 582-612.
19. P. Makam and E. Gazit, *Chemical Society Reviews*, 2018, **47**, 3406-3420.
20. S. Zhang, *Nature biotechnology*, 2003, **21**, 1171-1178.
21. Z. Fan, L. Sun, Y. Huang, Y. Wang and M. Zhang, *Nature Nanotechnology*, 2016, **11**, 388-394.
22. M. Şardan Ekiz, G. Cinar, M. Khalily and M. Guler, *Nanotechnology*, 2016, **27**, 402002.
23. L. Adler-Abramovich, M. Reches, V. Sedman, S. Allen, S. Tendler and E. Gazit, *Langmuir : the ACS journal of surfaces and colloids*, 2006, **22**, 1313-1320.
24. M. Lansalot and J. Rieger, *Macromolecular Rapid Communications*, 2019, **40**, 1800885.
25. N. Penfold, J. Yeow, C. Boyer and S. Armes, *ACS Macro Letters*, 2019, **8**, 1029-1054.
26. C. Ferguson, R. Hughes, B. Pham, B. Hawkett, R. Gilbert, A. Serelis and C. Such, *Macromolecules*, 2002, **35**, 9243.
27. V. Cunningham, A. Alswieleh, K. Thompson, M. Williams, G. Leggett, S. Armes and O. Musa, *Macromolecules*, 2014, **47**, 5613-5623.
28. M. Derry, L. Fielding and S. Armes, *Polym. Chem.*, 2015, **6,** 3054-3062.
29. M. Semsarilar, V. Ladmiral, A. Blanazs and S. P. Armes, *Langmuir*, 2012, **28**, 914-922.
30. A. Blanazs, J. Madsen, G. Battaglia, A. Ryan and S. Armes, *Journal of the American Chemical Society*, 2011, **133**, 16581-16587.
31. A. Blanazs, A. Ryan and S. Armes, *Macromolecules*, 2012, **45**, 5099–5107.
32. P. Chambon, A. Blanazs, G. Battaglia and S. Armes, *Macromolecules*, 2012, **45**, 5081–5090.
33. M. Semsarilar, V. Ladmiral, A. Blanazs and S. P. Armes, *Langmuir*, 2013, **29**, 7416-7424.
34. S. Boissé, J. Rieger, B. Khaled, A. Di-Cicco, P. Beaunier, M.-H. Li and B. Charleux, *Chemical communications (Cambridge, England)*, 2010, **46**, 1950-1952.
35. I. Chaduc, A. Crepet, O. Boyron, B. Charleux, F. D'Agosto and M. Lansalot, *Macromolecules*, 2013, **46**, 6013-6023.
36. W. Zhang, F. D'Agosto, O. Boyron, J. Rieger and B. Charleux, *Macromolecules*, 2011, **44**, 7584-7593.
37. I. Chaduc, W. Zhang, J. Rieger, M. Lansalot, F. D'Agosto and B. Charleux, *Macromolecular rapid communications*, 2011, **32**, 1270-1276.
38. M. Derry, L. Fielding and S. Armes, *Progress in Polymer Science*, 2016, **52**, 1-18.
39. M. Semsarilar, V. Ladmiral, A. Blanazs and S. Armes, *Polym. Chem.*, 2014, **5**, 3466-3475.
40. M. Semsarilar, N. Penfold, L. Jones and S. Armes, *Polym. Chem.*, 2015, **6**, 1751-1757.
41. X. Zhang, J. Rieger and B. Charleux, *Polym. Chem.*, 2012, **3**, 1502-1509.
42. L. Fielding, J. Lane, M. Derry, O. Mykhaylyk and S. Armes, *Journal of the American Chemical Society*, 2014, **136**, 5790-5798.
43. A. Lopez-Oliva, N. Warren, A. Rajkumar, O. Mykhaylyk, M. Derry, K. Doncom, M. Rymaruk and S. Armes, *Macromolecules*, 2015, **48**, 150522153344002.
44. Q. Zhang and S. Zhu, *ACS Macro Letters*, 2015, **4**, 755-758.
45. D. Zhou, R. Kuchel, S. Dong, F. Lucien, S. Perrier and P. Zetterlund, *Macromolecular Rapid Communications*, 2018, **40**, 1800335.
46. T. P. T. Dao, L. Vezenkov, G. Subra, M. Amblard, M. In, J.-F. Le Meins, F. Aubrit, M.-A. Moradi, V. Ladmiral and M. Semsarilar, *Macromolecules*, Submitted.
47. V. Ladmiral, M. Semsarilar, I. Cantón and S. Armes, *Journal of the American Chemical Society*, 2013, **135**, 13574-13581.
48. N. Warren and S. Armes, *Journal of the American Chemical Society*, 2014, **136**, 10174-10185.
49. L. Adler-Abramovich, L. Vaks, O. Carny, D. Trudler, A. Magno, A. Caflisch, D. Frenkel and E. Gazit, *Nature chemical biology*, 2012, **8**, 701-706.

Nano-assemblies with Core-Forming Hydrophobic Polypeptide *via* Polymerization-Induced Self-Assembly (PISA)

T. P. Tuyen Dao[a,b,c], Lubomir Vezenkov[c], Gilles Subra[c], Vincent Ladmiral[b], Mona Semsarilar[a*]

a. Institut Européen des Membranes, IEM, Univ Montpellier, CNRS, ENSCM, Montpellier, France
b. Institut Charles Gerhardt Montpellier, ICGM, Univ Montpellier, CNRS, ENSCM, Montpellier, France
c. Institut des Biomolécules Max Mousseron, IBMM, Univ Montpellier, CNRS, ENSCM, Montpellier, France

SUPPORTING INFORMATION

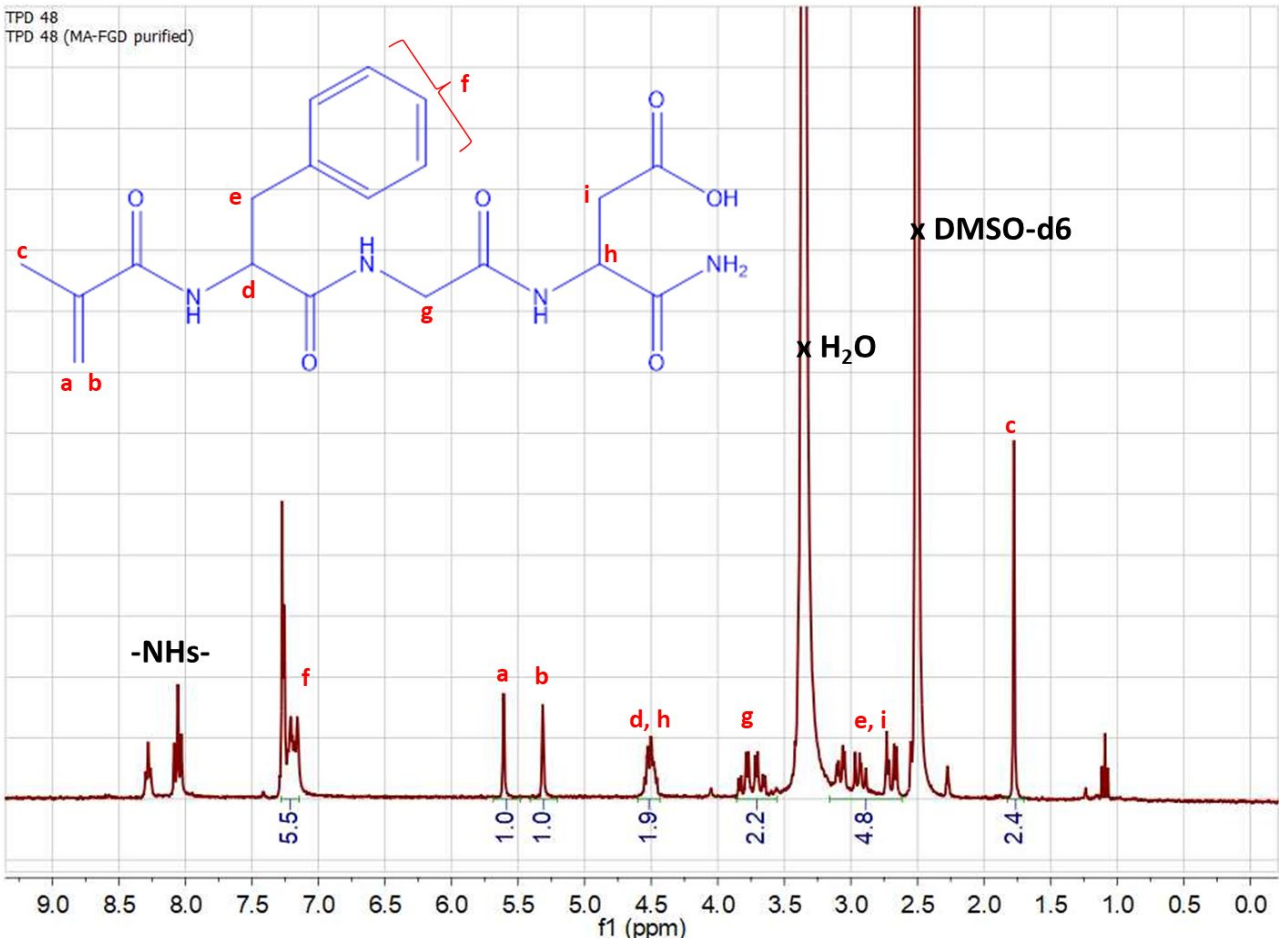

Figure S1. Chemical structure and ^{1}H NMR spectrum in DMSO-d6 of MAm-FGD

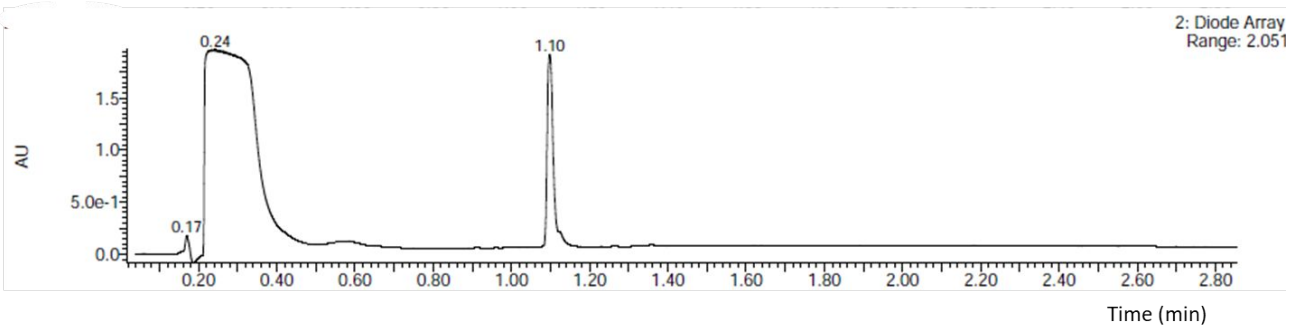

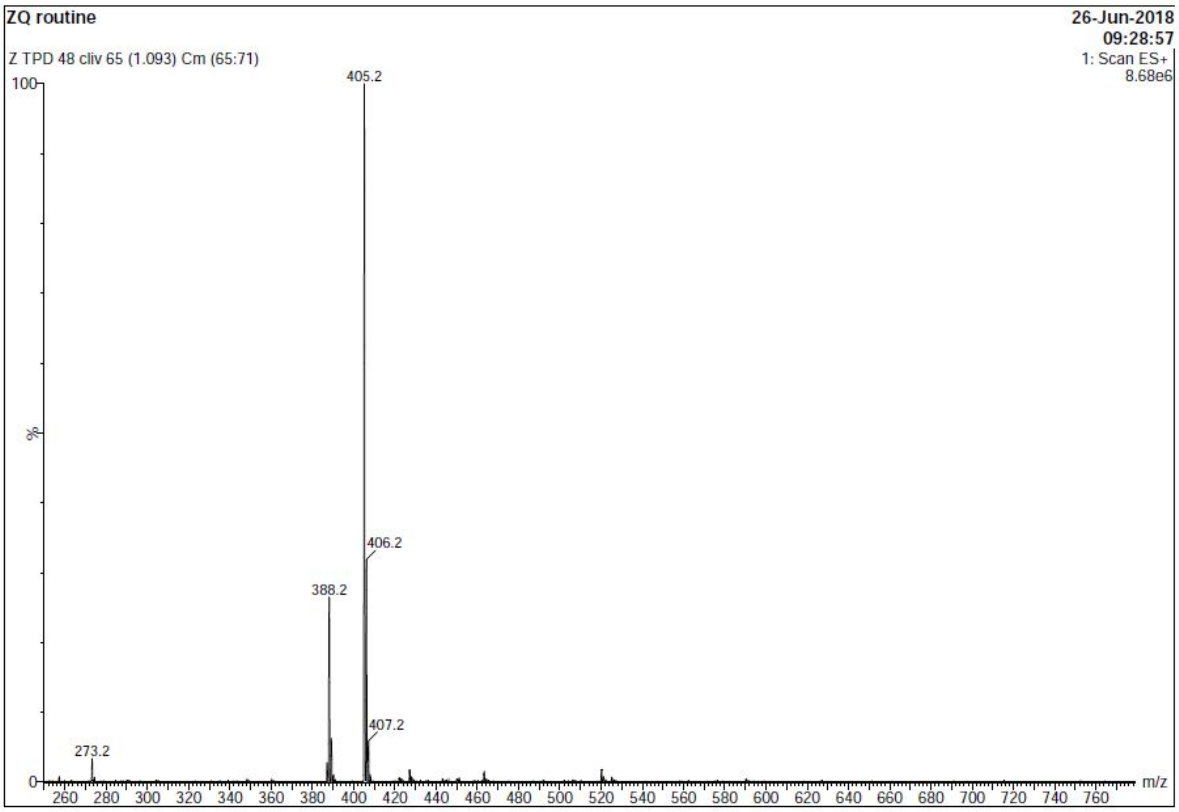

Figure S2. HPLC profiles and ESI-MS of MAm-FGD (t_R = 1.10 min, m/z 405.2 ([M+H]$^+$))

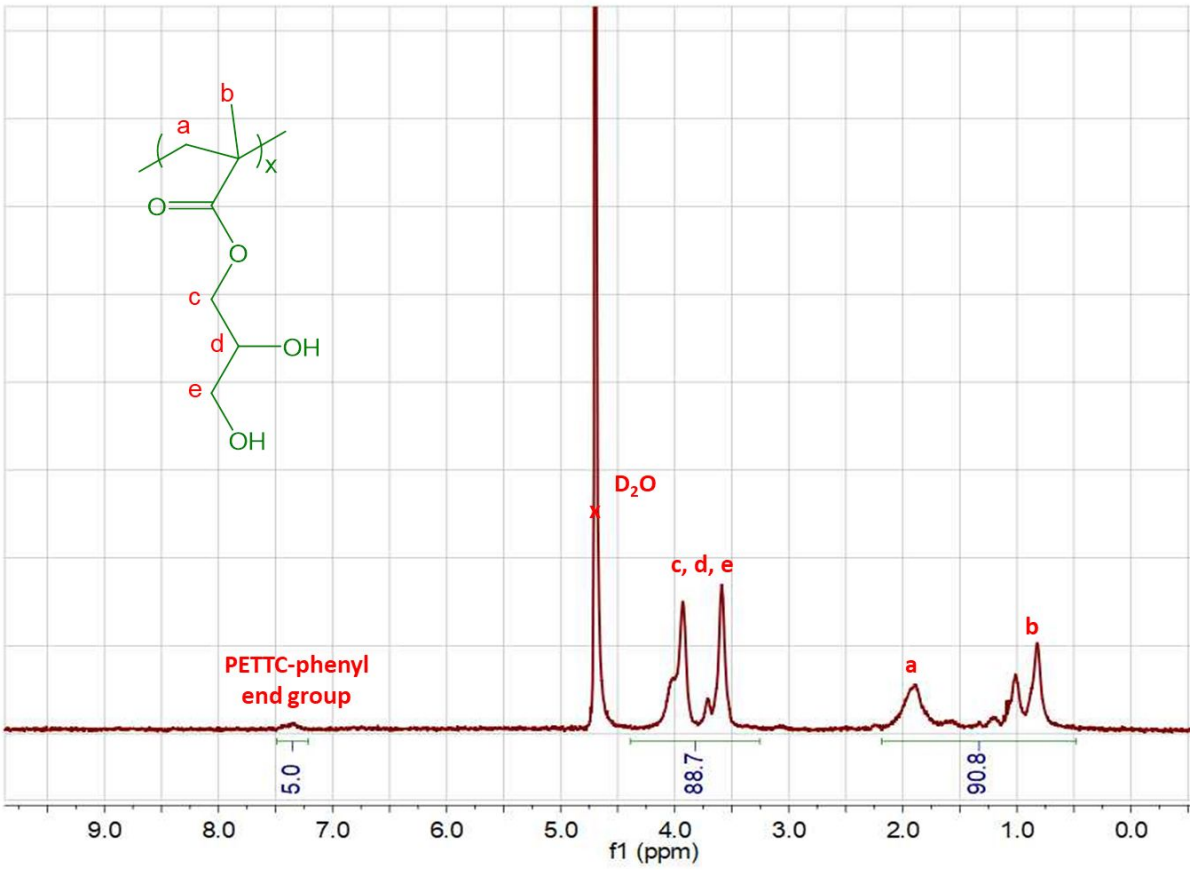

Figure S3. Chemical structure and ^{1}H NMR spectrum in D_2O of $PGMA_{18}$ mCTA (mCTA **1**)

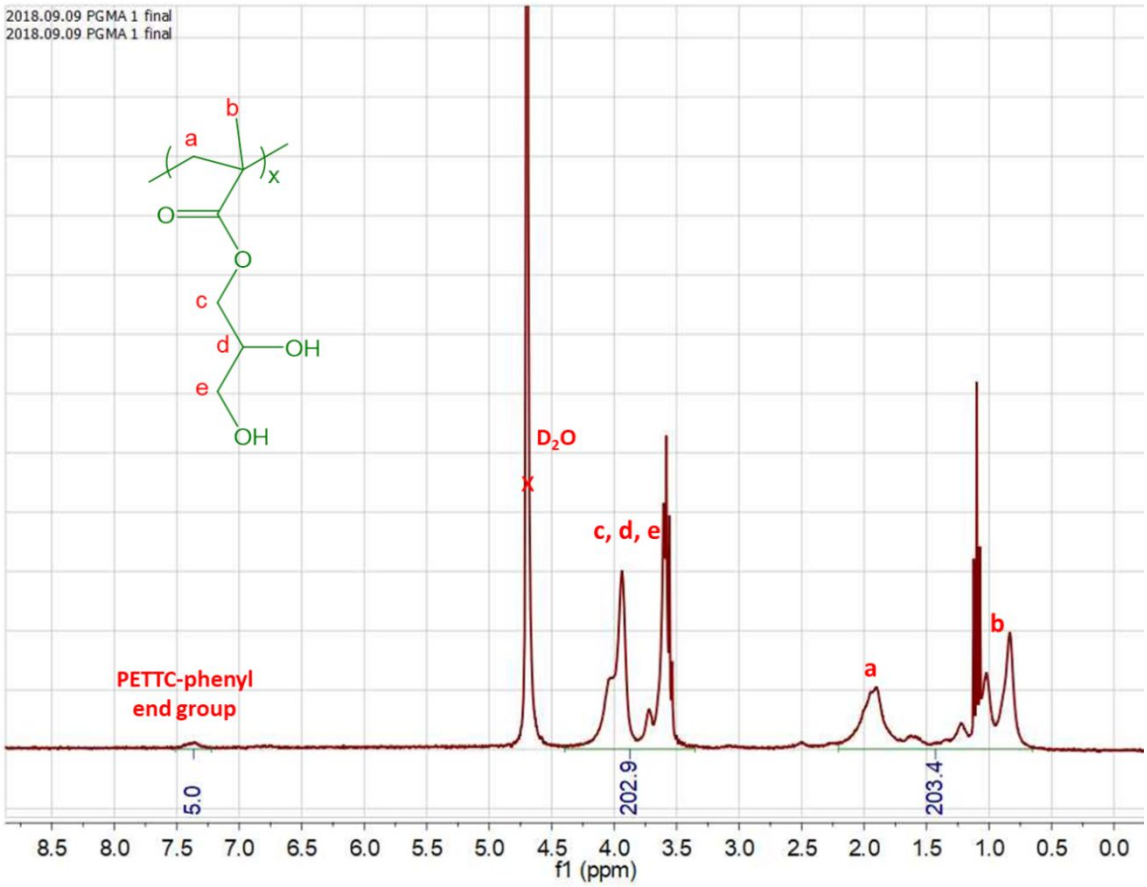

Figure S4. Chemical structure and ^{1}H NMR spectrum in D_2O of $PGMA_{40}$ mCTA (mCTA **2**)

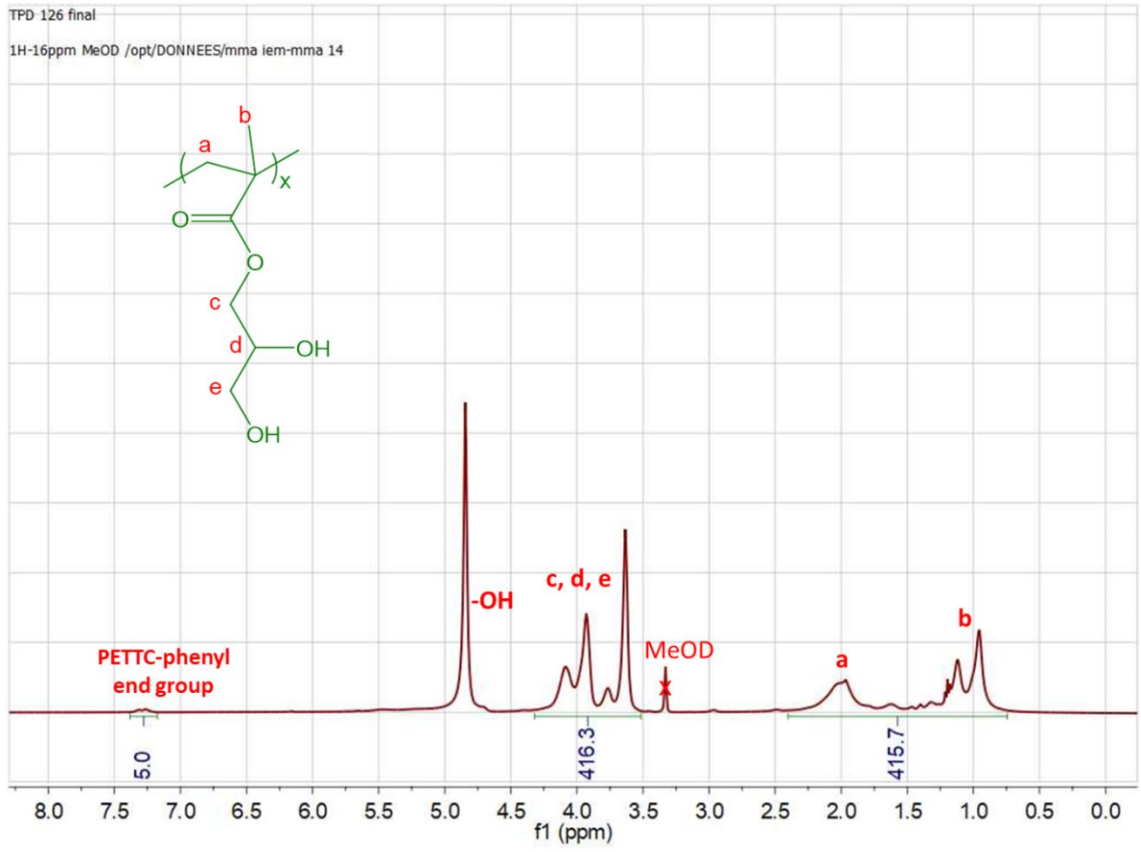

Figure S5. Chemical structure and ^{1}H NMR spectrum in Methanol-d4 of $PGMA_{83}$ mCTA (mCTA **3**)

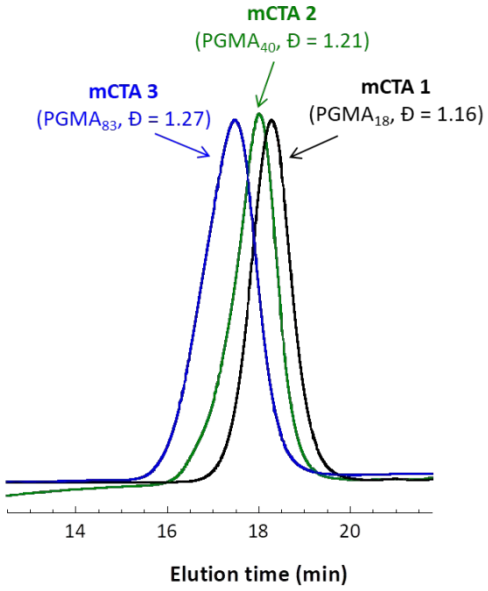

Figure S6. DMAc SEC data (refractive index detector) for the PGMA macro-CTAs

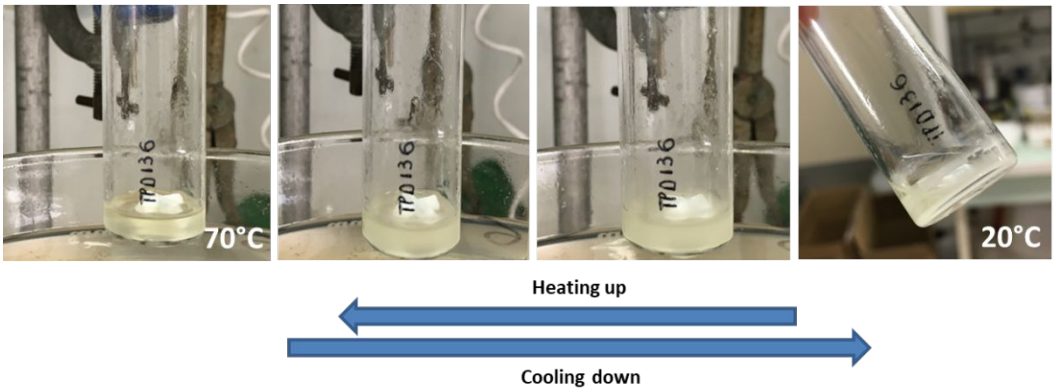

Figure S7. Photos taken for diblock copolymer $PGMA_{18}$-*b*-$P(MAm\text{-}GFF)_4$ obtained by PISA carried out at 11.2 % w/w in ethanol at 70°C and when cooling down to ambient temperature (ca. 20°C)

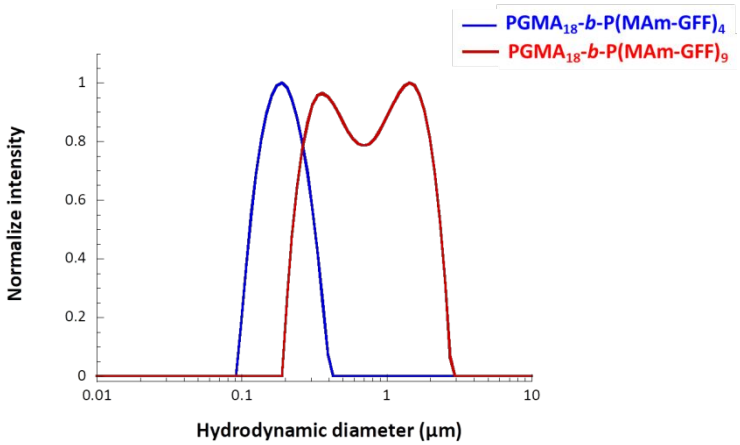

Figure S8. Intensity-average hydrodynamic diameter distribution of $PGMA_{18}$-*b*-$P(MAm\text{-}GFF)_4$ and $PGMA_{18}$-*b*-$P(MAm\text{-}GFF)_9$ suspension in ethanol at 0.112 % w/w and 0.125 % w/w repsectively

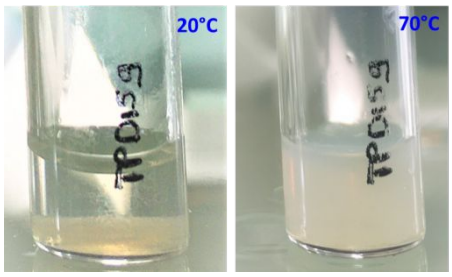

Figure S9. Diblock copolymer $PGMA_{18}$-*b*-P((MAm-GFF)$_9$-*co*-GMA_{48}) obtained by PISA carried out at 15% w/w in ethanol at 70°C: on the left: after cooling from 70°C to 20°C and on the right: heating it up again from 20°C to 70°C (right)

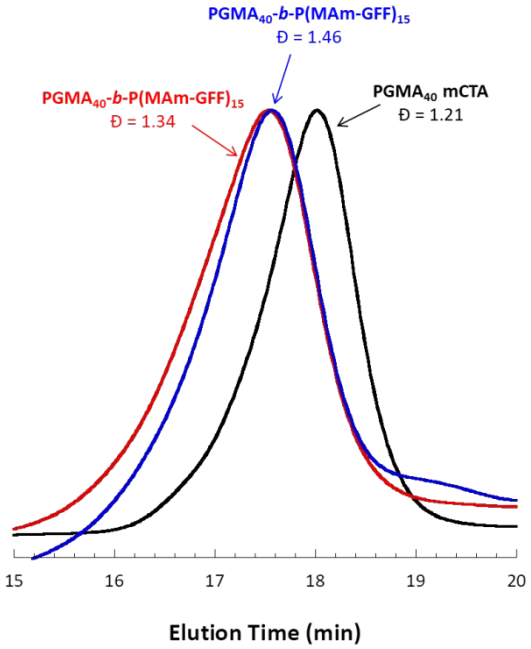

Figure S10. DMAc SEC chromatograms (refractive index detector) of mCTA 2 ($PGMA_{40}$) and diblock copolymers $PGMA_{40}$-*b*-P(MAm-GFF)$_{15}$ prepared *via* RAFT-mediated PISA in 1/1 v/v and 1/2 v/v water/acetonitrile mixtures (red and blue respectively)

Table S1. Summary of the conditions and results of RAFT-PISAs to synthese the diblock copolymers in this work

Products	Solvent	Visual aspect at starting time of PISA (at 70°C)	Solids content (%)	Initial ratio $[mCTA]_0$: $[peptide]_0$: $[ACVA]_0$ or $[mCTA]_0$: $[peptide]_0$: $[GMA]_0$: $[ACVA]_0$ or $[mCTA]_0$: $[peptide]_0$: $[HPMA]_0$: $[ACVA]_0$	Monomer peptide conversion (%)	Đ $_{GPC}$ (DMAc)	Visual aspect at ending time of PISA (at 70°C)
Macro-CTA 1: $PGMA_{18}$	-	-	-	-	-	1.16	-
$PGMA_{18}$-*b*-P(MAm-GFF)$_4$	Ethanol	Solution	5%	1 : 5 : 0.2	45%	-	Clear solution
$PGMA_{18}$-*b*-P(MAm-GFF)$_4$	Ethanol	Emulsion	11.2 %	1 : 5 : 0.2	87%	1.17	Turbid suspension
$PGMA_{18}$-*b*-P(MAm-GFF)$_9$	Ethanol	Emulsion	12.5 %	1 : 10 : 0.2	92%	1.28	Turbid suspension
$PGMA_{18}$-*b*-P((MAm-GFF)$_9$-*co*-GMA_{48})	Ethanol	Emulsion	15%	1 : 10 : 48 : 0.2	90%	1.33	Turbid suspension

$PGMA_{18}$-*b*-P(($MAm\text{-}GFF)_9$-*co*-$HPMA_{61}$)	Ethanol	Emulsion	15%	1 : 10 : 61 : 0.2	90%	1.38	Clear dispersion
$PGMA_{18}$-*b*-P(($MAm\text{-}GFF)_{19}$-*co*-$HPMA_{50}$)	Ethanol	Emulsion	15%	1 : 20 : 50 : 0.2	95%	1.32	Clear dispersion
$PGMA_{18}$-*b*-P$(MAm\text{-}FGD)_{10}$	Water	Solution	10%	1 : 10 : 0.2	100%	1.24	Turbid suspension
Macro-CTA 2: $PGMA_{40}$	-	-	-	-	-	1.21	-
$PGMA_{40}$-*b*-$PMAGFF_8$	Ethanol	Emulsion	12%	1 : 10 : 0.2	86%	1.34	Turbid suspension
$PGMA_{40}$-*b*-$PMAGFF_{15}$	H_2O/ACN 1/1 v/v	Solution	10%	1 : 20 : 0.2	69%	1.34	Clear dispersion
$PGMA_{40}$-*b*-$PMAGFF_{15}$	H_2O/ACN 1/2 v/v	Solution	10%	1 : 20 : 0.2	72%	1.46	Clear dispersion
$PGMA_{40}$-*b*-P$(MAm\text{-}FGD)_{20}$	Water	Solution	10%	1 : 20 : 0.2	100%	1.24	Turbid suspension
Macro-CTA 3: $PGMA_{83}$	-	-	-	-	-	1.27	-
$PGMA_{83}$-*b*-$PMAGFF_6$	Ethanol	Emulsion	12%	1 : 6 : 0.2	90%	1.26	Turbid suspension
$PGMA_{83}$-*b*-$PMAGFF_{10}$	Ethanol	Emulsion	12%	1 : 10 : 0.2	95%	1.42	Turbid suspension
$PGMA_{83}$-*b*-P$(MAm\text{-}FGD)_{20}$	Water	Solution	10%	1 : 20 : 0.2	100%	1.29	Clear dispersion